THE UNIVERSITY OF MANITOBA

PRECIPITATION BEHAVIOUR OF A NEW COBALT-CHROMIUM-NICKEL SUPERALLOY

by

DONG WHA CHUNG

A THESIS

SUBMITTED TO THE FACULTY OF GRADUATE STUDIES

IN PARTIAL FULFILLMENT OF THE REQUIREMENTS FOR THE DEGREE

OF

MASTER OF SCIENCE

DEPARTMENT OF MECHANICAL ENGINEERING

WINNIPEG, MANITOBA

October, 1972

PRECIPITATION BEHAVIOUR OF A NEW COBALT-CHROMIUM-NICKEL SUPPERALLOY

CONTENTS

1.0 INTRODUCTION

Superalloys are complex materials and are extensively used in high temperature applications because of their good mechanical properties and corrosion resistance. In nickel based superalloys the matrix phase, γ, is a solid solution of various elements and maintains a F. C. C. structure. These superalloys also contain Al, Ti, Nb which form a fine dispersion of γ' phase, Ni_3 (Al, Ti, Nb). Most of the strength of superalloys is derived by the precipitation of γ' phase. Cobalt based superalloys can provide a better hot corrosion resistance, have a flatter stress-rupture/time temperature parameter, also they can be used at temperatures a few hundred degrees higher than nickel alloys (1). Cobalt also increases the solubility temperature of γ', thus increasing the maximum temperature at which an alloy can be used (2). Further increase in service temperature can be obtained by the addition of increased amounts of Ti and Al (2).

Based on these factors the following alloy was developed.

Co 38-45%, Ni 38-45%, Cr 16-20%, (Ti + Al) Balance.

It has been observed that in nickel based alloys containing Ti, addition of Al is not necessary to obtain γ' precipitate (3-5). Therefore, studies of the following Al-free alloy were initiated for the present investigation.

40 wt% Co, 38 wt% Ni, 17 wt% Cr, 5 wt% Ti.

2. REVIEW OF THE LITERATURE

2.1 Precipitation Process

Many earlier works have established that on aging supersaturated alloys tend to precipitate out the excess vacancies and solute atoms. The structural change during aging may also involve the precipitation of intermediate phases before the formation of the equilibrium precipitate occurs.

When a precipitation hardenable alloy is rapidly quenched from the single phase into the two phase regions of the equilibrium diagram (Fig. 1) considerable supersaturation of both solute atoms and vacancies occurs. This supersaturation can amount to a factor of ten or more for the solute, while for vacancies supersaturation ratios of perhaps 10^{10} can be obtained (6. 7. 8).

It was indicated that aging following a quench from the solution temperature (quench - aging) the solute supersaturation could be relieved only along with a concomitant relief in the supersaturation of vacancies. Furthermore, if there is a nontrivial energy of interaction between solute and vacancy during substitutional diffusion, the supersaturation relieving process becomes coupled with solute atoms and vacancies. In such a situation, Herman (9) has indicated that vacancies can join to form another species which act to transport solute during precipitation reactions.

When a precipitate particle is formed in a matrix, the free energy change is composed of the algebraic sum of the volume free energy change, ΔGv, the surface free energy change, ΔGs, and the strain free energy change, ΔGe, $\Delta Gt = \Delta Gv + \Delta Gs + \Delta Ge$ (10). For the homogeneous nucleation in the supersaturated alloy, ΔGv will be negative and ΔGs and ΔGe will be positive since the precipitate particle is very small, the surface free energy term will dominate and may lead to the formation of a transition lattice.

As the particle grows, the volume free energy and the strain free energy terms dominate its total free energy. Thus a transition lattice, which may be stable when a particle is very small, becomes unstable as the particle enlarges. But when a particle has become large enough so that the surface and strain free energy terms overcomes the first, the particle will tend to transform to a crystal structure which is more stable, but which is surrounded by a higher energy interface than the previous coherent interface. Therefore, maximum strengthening of the alloy occurs just before the precipitate loses its coherency, because at that stage of particle growth coherency strains are at their highest level (11).

The free energy change for Heterogeneous Nucleation also can be derived from the same three terms as the equation for homogeneous nucleation. In general, there are two types of heterogeneous nucleation, which are nucleations on dislocations and at grain boundaries.

A dislocation can be able to partially or fully accommodate the lattice misfit of a precipitate particle (16). Therefore, dislocations can be favorable nucleation sites. Cahn (16) assumed that the effect of the dislocation is to reverse the sign of the strain energy term, and also derived the nucleation rate on dislocations is 10^{78} times the rate of homogeneous nucleation. But at the grain boundary, the ΔGs term in the equation of free energy for nucleation reduce while ΔGe may or may not be lowered. This results in a lowering of ΔGt at a grain boundary and thus provides a preferential nucleation site.

2.2 Precipitation of γ' Phase

The precipitation of γ' is by far the most important strengthening mechanism in Ni-base superalloys. This γ' (46) is an ordered, face-centered cubic phase having the LI_2 type of crystal structure and is based on Ni_3 Al. This precipitate has a low mismatch with the γ matrix and generally forms as small, coherent spheres or cubes.

In cobalt-base alloys, γ' precipitate has also been utilized, but this is a relatively recent development. However, factors to which attention has to be addressed in considering γ' precipitation are:

1. Nucleation
2. Mismatch with lattice and coherency
3. Coarsening behavior of the γ' phase
4. Transformation of γ' to a stable phase

Manenc (12. 13) and Williams (14) used x-ray techniques and electron-microscopy of replicas in studying the precipitation of γ' in binary Ni-Al alloys and concluded that a multistage process is involved. Manenc suggested a first stage of "preprecipitation", followed by precipitation of a coherent intermediate phase (on {100} planes) which was slightly tetragonal due to coherency strains, followed by a visible stable precipitate possessing the equilibrium F. C. C. structure.

Bagariatskii and Tiaphin (15) concluded that the initial precipitation structure consists of isolated G-P zones.

Ben Israal and Fine (4) followed a suggestion of Cahn (16) and postulated that γ' in Ni-Ti alloy is caused by spinodal decomposition.

Working with a Ni-12 Cr-37 Fe-6 Mo-3.22 Ti-0.26 Al-0.05C alloy, Hammond and Ansell (17) concluded that γ' particles have random crystallographic orientations and are incoherent with the matrix. They also suggested that γ' is heterogeneously nucleated on collapsed vacancy discs.

Ardell and Nicholson (18) showed that γ' precipitation is frequently found to have a modulated structure, both in the binary alloys of Ni-Al and also in commercial alloys. They have also shown that the modulated structure develops from an initially random precipitate distribution which gradually changes to one where cubic precipitates are aligned along <100> directions.

If the initial formation of γ' were due to spinodal decomposition, the modulation would be present from the very earliest stages of the aging sequence. Thus, for the small supersaturations of solute in Ardell and Nicholson's alloy, spinodal decomposition does not seem to play a role in the nucleation of γ'.

Phillips (19) has investigated a similar alloy and has again shown that spinodal decomposition is not responsible for the initial precipitation of γ'. He also showed that precipitation of γ' in Ni-Al alloy is not a multistage process but is a normal nucleation

and growth process. At high supersaturations coherent γ' precipitates by homogeneous nucleation and overages to a modulated structure.

At lower supersaturation (high aging temperature), Phillips has shown that localized precipitation of γ' on dislocations occurs. Recently Raynor (20) has concluded that dislocations can act as nucleation sites for precipitation of faulted γ', and this occurs only when γ' is unstable with respect to the η (hexagonal) phase, i. e. in alloys with high Ti: Al ratios.

The shape of individual γ' precipitates varies from perfect spheres to perfect cubes, although most particles have some intermediate shape. Hagel and Beattie (21) have suggested that spheres are formed when the lattice misfit between γ' and the matrix is less than ~ 0.5%, and cubes are formed in the range of 0.5 to 1.0%, but when the disregistry is greater than ~ 1.0%, γ' precipitation is inhibited and discontinuous precipitation occurs. Heslop (22) has shown that in Nimonic alloy 115 a cubical γ' phase occurs and the misfit is less than 1.0%. Kelly and Nicholson (23) have suggested that the shape effect on increasing size (the lattice mismatch) may be associated with the loss of coherency of the particle at an intermediate stage in the aging process. However, analysis of diffraction effects from thin foil studies (24) on a binary Ni-Al alloy indicated that such "loss of coherency" does not necessarily occur when γ' particles cease to be spherical.

For small spherical particles with only one "g" (the reciprocal lattice vector) operating, the Ashby-Brown (25) theory predicted (Fig. 2) that a line of no contrast will occur perpendicular to "g" for small coherent particles due to the strain field around the coherent particles. For larger particles, Ardell (24) has shown that the strain contrast takes the form of "δ-fringes": (which are anti-symmetrical (the extreme fringes are of opposite type) in bright field and symmetrical in dark field (24), in contrast with stacking-fault or α-fringes which are symmetrical in bright field and anti-symmetrical in dark-field (48)) The fact that the large particles are still coherent is borne out by the existance of the fringes. He has also shown that the width of the δ-fringe increases with increasing "g" vector.

Recently Sass and Cohen (26) by transmission electron microscopy studies have arrived at the conclusion that γ' in Ni-Ti alloys is itself preceeded by another metastable precipitate with a composition approximating to Ni6Ti. The kinetics of the γ' particle growth follows the Lifshitz-Wagner (27. 28) theory, within the limits of experimental error. According to Wagner's volume diffusion-controlled model (OSTWALD RIPENING), precipitate particle growth can be expressed by

$$(\bar{r}t)^3 - (\bar{r}_o)^3 = Kt$$

$$K = \frac{8.\gamma.D.Co.Vm^2}{9.R.T}$$

where

$\bar{r}_t$: average particle radius which is a function of time "t"

$\bar{r}_o$: particle radius at the onset of coarsening

D: the diffusivity of solute

Co: the concentration of solute in the matrix

Vm: the particle molar volume

γ: the surface tension

R: gas constant

T: absolute temperature

K: a rate constant

In studies of the kinetics of precipitate growth, it is usual to examine the behavior of $\bar{r}$ with time: $(\bar{r}_t)^3$ proportional to "t" provides evidence that Ostwald ripening has occurred. Wagner further showed that the size distribution of the precipitate radii; r, was given by

$$W(\rho) = \frac{\text{constant}}{(1 + t/\Gamma)^{3/4}} \quad \rho^2 \left(\frac{3}{3 + \rho}\right)^{7/3} \left(\frac{3/2}{3/2 - \rho}\right)^{11/3} \quad \exp\left(\frac{-\rho}{3/2 - \rho}\right)$$

where $\rho = r/\bar{r}$

This expression describes a bell-shaped distribution skewed toward larger particle sizes and falling to zero at = ρ = 3/2

The constant is defined as

$$\Gamma = \frac{9(\bar{r}o)^3 \cdot R \cdot T}{8\gamma \cdot D \cdot Co \cdot Vm^2}$$

For cube-shaped γ' particles, Ardell (29) has proposed the following relation

$$(\bar{a}/2)^3 - (\bar{a}o/2) = K't \qquad K' = \frac{8\gamma CeDVm^2}{9RT}$$

Ce: concentration of solute in the matrix in equilibrium with an infinitely large γ' particle

Vm: molar volume of γ'

γ: specific free energy of the γ' - matrix interface

D: diffusion coefficient of titanium in nickel

$\bar{a}$: average particle size from edge lengths, a.

$\bar{a}o$: average edge length at "t" = 0 (the onset of coarsening).

Using this equation Ardell has found that the distribution of γ' particle sizes was significantly broader than the theoretical distribution of the Lifshitz-Wagner model. He also suggested that this was due to the relatively large lattice parameter mismatch between γ' and the Ni-Ti matrix.

2.3 Stable Intermetallic Precipitation

In an earlier work on Ni-Al alloy it has been observed by Williams (14), that during the isothermal aging there are two consecutive processes. The first was a change in atomic configuration resulting in increased short-range order, the second was formation of the actual precipitate Ni_3 Al and the discontinuous precipitation was incoherent. After long aging time the precipitates were cubes (30, 31) which tended to be grouped in rows parallel to the <100> axes (30) so that they appeared to be plate types when viewed in opaque sections at low magnification.

In austenitic iron-base alloy containing Ti (32), a cellular precipitation reaction after long aging time in which cells consisting of alternate lamellae of hexagonal Ni_3 Ti (47) (DO_{24} type of structure), austenitic γ, were formed. The habit plane of the Ni_3 Ti lamellae was

$$(001)\ Ni_3\ Ti\ //\ (111)\gamma;$$

$$[010]\ Ni_3\ Ti\ //\ [\bar{1}10]\ \gamma\ (32)$$

He also suggested that an almost perfectly coherent interface was formed between Ni_3 Ti lamellae with this orientation relationship and the intervening austenite. Another cellular reaction at grain boundaries in an austenitic steel containing Ti was observed by Singhal and Martin (33).

The interfacial structure of the broad faces of γ [(H.C.P.) Ag_2 Al] plates precipitated from α (F.C.C.) solid solution of Al-Ag alloy has

been studied by Laird and Aaronson (34). They found that all of these structures consist of a/2 [112] partials aligned primarily in an edge orientation. But Weatherly and Nicholson (35) have observed that the dislocation structure of γ' in Ni-Cr-Ti-Al alloy consists of hexagonal networks of a/2 [110] dislocations and that the mean spacing of misfit dislocations is consistant with the lattice parameter values. They have also concluded that the detailed shape of the precipitate, and the loss of coherency occurs by absorption of matrix dislocations into the interfaces.

3. EXPERIMENTAL TECHNIQUES

The composition of the alloy was (in wt%) 40%Co - 38%Ni - 17%Cr - 5%Ti, C less than o.01%.

The alloy was made in an argon arc furnace using 99.99% pure materials except Ti which was 99.7% pure.

3.1 Alloy Fabrication

The cold working of this alloy in the as-cast condition was extremely difficult. The ingots were first solution treated at 1250^{o}C for 60 hours and then rolled down from 0.8 inch to about 0.43 inch diam. rods. These were swaged to 0.200 inch rods with successive intermediate anneals at 1250^{o}C. Specimens for hardness measurements, optical microscopy and electrolytic extraction for x-ray analysis were cut from these rods. They were also rolled down to 0.005 inch thick strips at room temperature for thin film electron microscopic specimen preparation, with frequent intermediate anneals at 1250^{o}C.

3.2 Heat Treatment

All heat treatments were carried out with the specimens sealed off in argon-filled silica tubes.

The solution treatment was followed by an iced water quench. During quenching the silica tube was broken under water to minimize the precipitation reaction. It was observed that at 1250^{o}C this alloy had oxidized even under the reduced pressure of argon. The oxide

layer was removed by electropolishing after heat treatment.

Aging treatments were carried out at 700°C, 800°C, and 900°C for times up to 1200 hours.

3.3 Hardness Measurement and Optical Microscopy

A vickers pyramid hardness testing machine with a pyramid diamond indenter and 10 kilogram load was used for the hardness measurements. The average hardness values were obtained by making 12 indentations.

Before electron microscope studies, the overall structure was examined using a vicker's optical microscope and the hardness specimen.

3.4 Electropolishing and Etching

The specimen were electropolished at 10V in a bath of 10% sulfuric acid, 90% methanol which was maintained at just below 0°C and stirred slowly. After polishing for 8 to 10 minutes, the specimen was quickly washed in running water and then dried with absolute alcohol, since titanium in the alloy is liable to form an oxide, which could be avoided by quick and careful drying.

The etching reagant used was 30 ml lactic acid, 20 ml hydrochloric acid, 10 ml nitric acid for γ' phase, and two parts HCl, three parts HNO_3, and four parts glycerine for an overaged specimen (η phase). After being etched, the specimen was quickly washed in alcohol, then in running cold water, and finally washed again in pure alcohol and dried.

Etching time and etchant required depended upon the heat treatment. The specimen was mounted flat on a glass slide and examined under a Vicker's optical microscope.

3.5 Carbon Extraction Replica Techniques

After the etching process, a thin film of carbon was evaporated on the specimen. It was then electro-etched for a few seconds in a solution of 5% sulfuric acid, 95% methanol with 10 volts, until the carbon layer was loosened. The exact etching time was dependent on the particle sizes. When the γ' phase was extracted, care had to be taken to keep the particles on the carbon layer. After carefully washing in alcohol, the carbon film was floated in a disc of distilled water and collected on a 200 mesh copper grid and then dried in air.

3.6 Thin Foil Technique

The electrolytic jet polishing technique was used to prepare thin foils. Heat treated 0.005 inch thick x 0.25 inch square strip was carefully polished mechanically and its edges were then lacquered. The specimen was then mounted anodically in a jet polishing cell. The bath contained 10% perchloric acid and 90% methanol, and was maintained at a temperature of $-50^{o}C$. The specimen was polished at 10 - 15 volts until a hole appeared. After a hole appeared the specimen was quickly removed from the electrolyte and put in cold alcohol for washing, cleaned of lacquer, rewashed in alcohol and

dried between filter paper. After drying, the specimen was held between two clean tissue papers and a suitable area was cut out with a sharp knife.

Care had to be taken in handling the specimen to avoid deformation. The thin foil was mounted in between two "100" mesh copper grids and examined in a Phillips E. M. 300 Microscope.

3.7 Electrolytic Extraciton for X-Ray Investigation

An extraction cell containing an electrolyte composed of 10% acetic acid in water was used to extract the preciptate particles at a current density of about 0.05 A/Cm^2. The extraction was carried out for 10 hours to extract sufficient amount of precipitate particles. After the matrix was completely dissolved in the solution, the solvent was removed by suction pump and the precipitate particles were washed in distilled water and in alcohol and successively dried. The well dried extracted particles were spread out on a clean paper and mounted in a thin glass tube with glue. The thin glass tube was mounted in a Phillips powder camera and irradiated by the Co $K\alpha$ radiation using an Fe filter. In order to obtain the value of the lattice misfit between matrix and precipitate, the lattice parameter of the matrix austenite and that of the precipitate were measured from the quench-aged powder sample and the extracted particles. Both specimens were exposed and the lines were indexed and the lattice parameters were calculated.

In order to obtain the true lattice parameter it was necessary to extrapolate the obtained values of the lattice parameters from each independent lines, as a function of the angle 2θ to a value for $2\theta = 180^{o}$.

4. RESULTS

The specimens were solution treated at 1250°C and quenched in iced water. The as-quenched structure of the alloy was austenitic (F. C. C.) as shown in figure 3. Occasionally some precipitation was also detected at grain boundaries which could not be identified. However, no precipitation within the grain was observed. The lattice parameter of the as-quenched specimen was determined by x-ray powder technique and was calculated to be 3.5513 Å. The solution treated specimens were aged at 700°, 800° and 900°C for various lengths of time. The aging kinetics at different temperatures of aging were followed by hardness measurements. Figure 4 shows the variation in hardness at different temperatures with aging time. It is seen that this alloy displays the normal aging behaviour i. e., as the aging temperature is reduced the time required to attain peak hardness and the hardness value at the peak are increased. However, at 700°C even after 1300 hours of aging peak hardness has not been achieved.

Various phases in the aged specimens were studied, mainly, by electron microscopy. The results of these studies will be presented in two sections viz., precipitation within the grains and precipitation at or near the grain boundaries.

4.1 Precipitation within the Grains

Only two phases were observed within the grains, γ' precipitate which is an ordered F. C. C. Ni_3 Ti and a hexagonal η Ni_3 Ti phase.

4.1.1 γ' - Phase

The precipitation characteristics of γ' phase at 700°C are essentially the same as those observed at 800 and 900°C. However, the stability of γ' is reduced as temperature of aging is increased to 900°C. In the early stages of aging γ' particles are coherent with the matrix and the structure appears to be modulated. Fig. 5 shows the structure and the diffraction pattern of a specimen aged for 30 minutes at 800°C. Diffraction pattern of an area from within the grain shows that the foil orientation is (110) and it also contains (001) reflection which is forbidden for an f. c. c. structure. This indicates the presence of γ' precipitate which has an ordered $Cu_3 Au$ type of structure. The presence of γ' was also confirmed by x-ray powder technique and its lattice parameter was calculated to be 3.5750Å. At this stage the strain field around γ' particle can not be resolved and it is not possible to apply the analysis due to Sass et al (36) to determine the shape of the precipitate particles. The earliest stage at which the shape of the particles could be determined with any degree of certainty was after two hours of aging at 800°C. Figure 6 shows a dark field electron micrograph of a specimen aged for two hours at 800°C. This dark field was taken with the help of (001) γ' superlattice reflection to eliminate contrast effects due to the coherency strains in the matrix. The shape of the particles appears to be cubic and they are about 100 Å in size. Also, they seem to be aligning themselves in <100> directions.

On further aging γ' particles grow in size while maintaining their cubic shape. The alignment of particles in <100> direction also becomes very pronounced.

The lattice parameter of the matrix of specimens aged for various lengths of time at 800^{o}C was measured by x-ray powder technique. The variation in the lattice parameter with the aging time is shown in figure 7. It is observed that the lattice parameter of γ decreases linearly with time for the initial 60 minutes of aging and then remains constant. This would indicate that the precipitation of Ti atoms from the matrix, for the formation of γ', takes place only during the early stages of aging. The growth of γ' phase on further aging occurs by volume diffusion at a constant volume fraction of γ' phase. Figure 7 shows the variation in the lattice parameter of γ', embedded in matrix as well as that of the electrolytically extracted, with aging time at 800^{o}C. It is seen that during the early stages of aging the lattice parameter of γ', embedded in matrix as well as chemically extracted, increases with the aging time and then remains constant. Also, the lattice parameter of electrochemically extracted γ' is greater than that embedded in matrix. However, in the overaged condition the lattice parameter of γ' embedded in the matrix approaches the value of the electrochemically extracted precipitate particles.

4.1.2 Transformation of γ' to Ni_3 Ti Hexagonal η Phase

As the aging process is continued γ' particles that were aligned in <100> directions start to coalesce into long straight rows. They also start to loose coherency which gives rise to interfacial dislocation around γ' particles. A typical thin film structure of a specimen aged for 575 hours at 800°C is shown in figure 8. The foil orientation of this micrograph is (123) and (111) is the operating reflection. It is seen that some of the γ' particles (area marked A) exhibit stacking fault fringe contrast. Figure 9 shows the bright and dark field micrographs of this area at a higher magnification. It is also observed that the trace of the plane of the stacking fault and the foil plane (123) is $[\bar{5}\bar{2}3]$ suggesting that the stacking fault is lying on the $(1\bar{1}1)$ plane. By the method of Gever et al (37) these faults were found to be intrinsic in nature.

On further aging coalesced γ' particles with interfacial dislocations start to transform to hexagonal Ni_3 Ti η phase with lattice parameter, $a = 5.122 \pm 0.005$ Å, $C = 8.242 \pm 0.001$Å. This is shown in figure 10 which is the thin film microstructure of a specimen aged for 650 hours at 800°C. The selected area diffraction pattern of this structure is shown in figure 11. The foil plane is (110), and the precipitate within the rows of γ' lie on {111} planes as the traces of the precipitate and the foil plane are $[1\bar{1}2]$ and $[\bar{1}12]$.

Because of the thinness of the precipitate ($20\bar{2}2$) hexagonal spot is seen to streak in (002) matrix direction and the direction of streaking is perpendicular to the precipitate. The satellite spots around (111) spots are typical of (111) habit as observed by Hirsch et al (37). Figure 11 shows the dark field micrograph of figure 10 taken with the help of ($\underline{20\bar{2}2}$) hexagonal reflection. This suggests that the dark needle shape particles seen within the rows of γ' particles are Ni_3 Ti hexagonal η phase. The above observations show that on continued aging γ' particles transform to stable hexagonal η phase. The nucleation of η phase seems to occur on stacking faults, within the γ' particles, which are instrinsic in nature.

On overaging the η phase grows by the transformation of remaining γ' phase and then coalesce to give rise to long thin plates of η phase. These plates grow at the expense of the adjacent γ' particles. Figure 13 shows the structure of a specimen aged for 1200 hours at $800^{o}C$. It is seen that long plates of η phase are surrounded by areas which are free from γ' precipitate particles. However, it was also observed that even after 1200 hours of aging some γ' had not yet transformed to η phase.

4.2 Precipitation on Grain Boundaries

Extensive precipitation was observed at or near grain boundaries at various temperatures of aging. The phases were identified as cellular Ni_3 Ti η phase, carbide phases and very limited amount of σ phase in the overaged specimen.

4.2.1 Carbide Phases

Mainly two types of carbide phases were identified viz., $M_{23}C_6$ type (F. C. C.) and TiC. Both precipitates were observed in the early stages of aging but only $M_{23}C_6$ type carbide was observed in the overaged specimens. Grain boundary precipitate in a specimen aged for 30 mins at 800°C, shown in figure 5 (A) was identified as $M_{23}C_6$ type carbide by the selected area diffraction technique (Fig. 14). $M_{23}C_6$ carbide at the grain boundary was also observed in a specimen aged for 30 mins at 700°C (Fig. 15) and 70 hours at 800°C (Fig. 19) as well as in well overaged specimens. TiC, however, was observed only in the early stages of aging. Figure 16 shows dark field micrograph of TiC precipitate at the grain boundary in a specimen aged for 7 hours at 800°C. On further aging TiC was not detected. Therefore, it seems that on overaging TiC transforms to $M_{23}C_6$.

4.2.2 Hexagonal Ni_3Ti η-phase

The grain boundaries also provide the nucleation sites for the precipitation of hexagonal η-phase. In the present alloy system this phase starts to precipitate at a very early stage of aging as shown at "X" in figure 15. This micrograph also shows the precipitation of $M_{23}C_6$ at the grain boundaries and γ' within the grains. As the aging progresses the cellular precipitation of η phase continues at the expense of γ' phase which has already precipitated out at a very early stage (Fig. 15). This mode of growth of η phase gives rise to a

γ' free zone around η plates and also a sharp η-γ' interface as shown in figure 17, which is the structure of a specimen aged for 70 hours at 800°C. The dark field micrograph of η phase is shown in figure 18. The fringes seen in the bright and dark field images of η plates are thickness fringes. The presence of $M_{23} C_6$ carbide at the grain boundary was also confirmed by dark field observations (Fig. 19). On further aging η plates continue to grow. The effect of increase in the aging temperature was only to increase the extent of cellular precipitation of η phase.

In addition to $Ni_3 Ti$ hexagonal phase, another cellular reaction was also observed at the grain boundaries. Thin film structure of this specimen is shown in figure 19, and a selected area diffraction pattern from area A is shown in figure 21. The diffraction spots in this pattern are due to γ, η and $(CoNi)_2 Ti$ phases (Fig. 22). $(CoNi)_2 Ti$ phase has an ordered face centered cubic structure, which is similar to $Cu_2 Mg$ type Lave phase. By electron diffraction analysis the lattice parameter of this phase was calculated to be 7.15 Å and seem to possess a cubic orientation relationship with the matrix. Repeated attempts fail to reveal this phase by x-ray powder analysis, which may be due to the very limited quantity of this phase being present.

4.2.3 σ - Phase

When aging was done at 900^{o}C the grain boundaries of the overaged specimen occasionally showed a leaf like precipitate, as observed in figure 23 which is the structure of a specimen aged for 300 hours at 900^{o}C. By electron diffraction technique (Fig. 24) this precipitate was found to be a tetragonal σ phase. The lattice parameters of this phase were calculated to be a = 8.40 Å, c = 4.48 Å and c/a = 0.533. Once again this phase was not observed by x-ray powder technique suggesting a very limited amount of σ phase being present.

5. DISCUSSION

The major precipitating phase in this alloy was observed to be γ', which has an ordered F. C. C. structure isomorphous with Ni_3 Al. The nucleation of γ' seems to be a homogeneous process as γ' particles were uniformly distributed throughout the matrix and no preferential nucleation on dislocation and defects was observed. Furthermore, when the cellular precipitation of η phase did not occur γ' particles were seen very close to the grain boundaries. If vacancies were playing a role in the nucleation of γ', a "precipitate-free" zone would be observed ground the grain boundaries (39, 40). In the absence of such a zone it may be concluded that vacancies are also not required for the nucleation of γ' and it is a homogeneous nucleation process.

The shape of γ' particles was established to be cubic in the size range of 100-500 Å by thin film dark field and carbon extraction replica techniques. The shape of the smaller particles could not be determined with any degree of certainty. The possibility of the particles being platelet in the early stages of aging and growing to cubic is ruled out because of the absence of any streaking in the electron diffraction patterns (Fig. 5). The smaller γ' particles could be spherical and acquire cubic shape during growth to 100 Å size, especially, since the cube faces show some rounding of the corners and apparent curvature of the faces (Fig. 6). In various Ni and Co base superalloys it has been observed that the shape of the γ' particles is spherical if the lattice mismatch between the matrix and γ' is 0.2 - 0.39% and cubic if it is 0.5 - 1.0% (21, 22). A lattice mismatch of 1.6% between the γ' matrix of the alloy aged at 800°C and the electrolytically extracted γ'

particles, formed at 800°C, was determined by x-ray lattice parameter measurements. However, the mismatch between γ' matrix and unextracted γ' was 1.3%. The cubic shape of the γ' phase with a lattice mismatch of 1.3% is in agreement with the previous findings (21, 22).

In the initial stages of aging the nucleation and growth of γ' phase occurs by the precipitation of Ti from the matrix solid solution. This results in a reduction of the lattice parameter of matrix (Fig. 7) as the atomic radius of Ti is larger than that of the matrix elements (Ti - 1.47 Å, Ni - 1.24 Å, Cr - 1.27 Å, Co - 1.25 Å). After about one hour at 800°C all the Ti atoms have precipitated out from the matrix. On further aging growth of γ' takes place by volume diffusion and the lattice parameter of γ remains constant. The lattice parameter of γ', embeded in the matrix as well as electrochemically extracted increases during the initial stages of aging (Fig. 7). This would suggest a lack of Ti atoms in γ' particles which might also prevent a complete ordering of the precipitate. As the amount of Ti reaches the required value the lattice parameter of γ' will attain the equilibrium value and will remain constant on further aging. The coherency strains in the matrix exert a hydrostatic compressive stress on the γ' particles, as a result; the lattice parameter of extracted γ' particles is observed to be greater than those embeded in the matrix (Fig. 7). On continued aging γ' particles start to lose coherency and the lattice parameter of γ embeded particles approaches that of electrolytically extracted γ' phase.

The hardness aging curve of the alloy at 800°C shows a plateau after one hour of aging. This plateau coincides with the range over which the growth of γ' phase occurs by volume diffusion and its volume remains constant. This mode of growth results in an increased γ' size and interparticle spacing. Therefore, the plateau in the hardness curve would indicate that during this period the yield strength of the alloy is only sensitive to the volume fraction of the precipitate phase and not the particle size and interparticle spacing. The drop in hardness curve seems to coincide with the partial loss of coherency of γ' particles and the start of the transformation of γ' to η phase.

The hexagonal η phase seems to form on {111} planes within the γ' particles that have coalesced into rows after about 500 hours of aging at 800°C. At this stage γ' particles also have a network of interfacial dislocations suggesting that they are only partially coherent (Fig. 8). The transformation of $\gamma' \rightarrow \eta$ seem to nucleate on stacking fault in the γ' particles. It has been suggested by Baker et al (41) that if the lattice parameter of the precipitate is greater than the matrix the coherent precipitate particles will be in a state of hydrostatic compression. The strain energy of such a system could be relieved by the condensation of a layer of vacancies on the close packed planes of the precipitate, which will produce an intrinsic fault within the precipitate. The hexagonal precipitate

can be considered as a F. C. C. structure with growth faculties on every other (111) plane. In the present alloy system the lattice parameter γ' is 1.6% greater than the matrix, therefore, the coherent precipitate particles experience a hydrostatic compression. The strain is partly relieved by the formation of an intrinsic fault, due to the condensation of vacancies on (111) γ' planes as suggested by Baker et al (41), and partly by the formation of interfacial dislocations as observed in Figure 8. These faults provide the nuclei for the formation of stable hexagonal phase (Fig.10). This mechanism is similar to that proposed by Meric and Nicholson (5) for the transformation of γ' - η phase in Ni-Cr-Ti alloy. The growth of η particle, on overaging, occurs by volume diffusion at the expense of surrounding γ' particles and results in a precipitate-free areas around η phase (Fig. 13).

The grain boundaries provide nucleation sites for the cellular precipitation of η phase, carbide and σ phases. The nucleation and growth of η phase seem to be similar to that observed in Ni-Ti-Cr (5), Ni-Al (14) and austenitic steels containing Ti (33, 32). The small amount of carbon that was present as an impurity gave rise to TiC and $M_{23}C_6$ type of carbides at the grain boundaries during early stages of aging. However, on continued aging only $M_{23}C_6$ was observed which would suggest that on overaging TiC transforms to $M_{23}C_6$. This transformation has been observed to occur by the diffusion of Ti

atoms from TiC to give rise to γ' and the carbon atoms from $M_{23}C_6$ as follows (42, 43).

$$MC + \gamma \rightarrow M_{23}C_6 + \gamma'$$

The σ phase was only observed very occasionally on overaging at 900°C. The PHACOMP analysis for predicting the formation of σ phase in superalloys (42-45), when applied to the present alloy system shows that the mean electron density number, $\bar{N}v$, of the residual matrix is 2.13. Therefore, according to PHACOMP analysis σ phase should not be observed. However, it is possible that the local variation in the matrix chemistry of the alloy around certain grain boundaries raises the value of $\bar{N}v$ over 2.52 and σ phase forms on overaging.

6. CONCLUSIONS

1. The main strengthening precipitate in the present alloy system is γ' which has an ordered F. C. C. structure. The nucleation of γ' occurs homogeneously throughout the matrix and the growth by volume diffusion at a constant volume fraction.

2. The lattice mismatch between γ' and the matrix is 1.3% and the particles have cubic shape. The cubic shape of γ' particles with this lattice mismatch is in agreement with the dependency of γ' particle shape on the lattice mismatch as observed in other super-alloys.

3. On overaging γ' transforms into stable hexagonal Ni_3 Ti - η phase. The nucleation of η phase occurs on intrinsic stacking faults within the γ' phase. The growth of η phase occurs at the expense of surrounding γ' particles.

4. The cellular precipitation of γ' phase, on the grain boundaries, also occurs. As the temperature of aging is raised the extent of cellular precipitation is also increased.

5. Carbon, which is present in the alloy as an impurity element, gives rise to TiC and M_{23} C_6 carbides. On continued aging TiC transforms to M_{23} C_6.

6. Occasionally, in the specimens overaged at 900°C, σ phase was also observed.

7. REFERENCES

1. C. T. Sims, J. Metals, 1969, Vol. 21, No. 12, p. 27.

2. G. P. Sabol and R. Stickler, Phys. Stat. Sol., 1969, Vol. 35, p. 11.

3. J. R. Mihalisin and R. F. Decker, Trans. Met. Soc. of A.I.M.E., 1960, Vol. 218, p. 507.

4. D. H. Ben Israel and M. E. Fine, Acta. Met., 1963, Vol. 11, p. 1051.

5. H. F. Merric and R. B. Nicholson, Fifth Int-Cong. Elec. Mic., Philadelphia, 1962, Vol. 1., p. K-8.

6. A. Guinier: Solid State Physics, Vol. 9, Academic press, New York, 1959, p. 293.

7. J. Friedal and A. Guinier, Metallic Solid Solutions: eds., Benjamin, New York, 1963.

8. A. Kelly and R. B. Nicholson: Prog. Mat. Scio, Vol. 10, pergamon press, London, 1963, p. 151.

9. Herbert Herman: Trans. A.I.M.E., Vol. 2, p. 13, 1971.

10. J. W. Christian, "Theory of Transformation of Alloys", 1965, Oxford and C. (pergamon press).

11. R. F. Mehl and L. K. Jetter, "The Mechanism of precipitation from solid solutions, The Theory of Age Hardening", Age Hardening of Metals, 1940, p. 342-417. American Society for metals.

12. J. Manenc, Rev. Met. (Paris), 54 (1967) 867.

13. J. Manenc, Acta. Met., 7 (1959) 124.

14. R. O. Williams, Trans, Met. Soc. A.I.M.E., 1959.

15. Yu A. Bagariatskii and Yu D. Tia Pkin, Soviet Phys. - Cryst, 2 (1957) 414.

16. J. W. Cahn, Acta Met., 9 (1961) 795; 10 (1962) 907; 5 (1957), 169.

17. C. M. Hammond and G. S. Ansell, Tran, Am. Soc. Metal, 57 (1964) 727.

18. A. J. Ardell and R. B. Nickolson, Acta Met., 14 (1966) 1295.

19. V. A. Phillips, Acta Met., 14 (1966) 1533.

20. D. Raynor, Met. Sci. Journal, 1971, Vol 5, Sep., p. 161.

21. W. C. Hagel and H. Beattie, Precipitation Processes in Steels, Iron and Steel Institute, London, 1959, p. 98.

22. J. Heslop, Cobalt, 24 (1964), p. 128.

23. A. T. Kelly and R. B. Nicholson, Progr. Mater. Sci., 10 (1963) p. 151.

24. A. J. Ardell, Phil. Mag., 16, (1967), p. 147.

25. M. F. Ashby and L. M. Brown, Phil. Mag., 8 (1963) 1083.

26. S. L. Sass and J. B. Cohen: Trans. TMS-AIME, 1969, Vol. 245, p. 153.

27. I. M. Lifshitz and V. V. Slyozov: J. Phys. Chem. Solids, 1969, Vol. 19, p. 35.

28. C. Wanger: Z. Elektrochem, 1961, Vol. 65, p. 581.

29. A. J. Ardell: Metallurgical Trans., Vol 1, 1970, p. 525.

30. V. A. Phillips, R. W. Guard and J. D. Livingston, Report ARL 62-357, U. S. Air Force, 1962.

31. B. E. P. Beeston and R. E. Smallman, Electron Microscopy 1964, Proc. Third Europ, Reg. Conf. on Electron Microscopy, Publ, H., of Czech. Acad. of Science, Prague, A. p. 165 (1964).

32. G. R. Speich, Trans A.I.M.E., 227, 1963, p. 754.

33. L. K. Singhal and J. W. Martin, J. Iron and Steel Inst., p. 947 (1967), Vol. 205.

34. C. Laird and H. I. Aaronson: Acta Met., Vol. 15, 1967, p. 73.

35. G. C. Weatherly and R. B. Nicholsen Phil. Mag., 1968, 17, 801.

36. S. L. Sass, T. Mura and J. B. Cohen, Phil. Mag., 1967, Vol. 16, p. 679.

37. R. Gevers, A. Art and S. Amelnckx, Phys., Stat. Sol., 1963, Vol. 3, p. 1563.

38. P. B. Hirsch, A. Howie, R. B. Nicholson, D. W. Pashley, and M. J. Whelan, "Electron Microscopy of Thin Cystals", Pub. Butterworths, 1965.

39. H. S. Rosenbaum and D. Turnbull, Acta. Met., 1958, Vol. 6, p. 653.

40. J. D. Embury and R. B. Nicholson, J. Aust. Inst. Metals, 1963, Vol. 8, p. 76.

41. R. G. Baker, D. G. Brandon, and J. Nutting, Phil. Mag., 1959, Vol. 4, p. 1339.

42. J. R. Mihalisin, C. G. Bieber and R. T. Grant, Trans. Met. Soc. A. I. M. E., 1968, Vol. 242, p. 239.

43. L. R. Woodyatt, C. T. Sims, H. J. Beattie, Jr., Trans. Met. Soc. A. I. M. E., 1966, Vol., 236, p. 519.

44. W. J. Boesch and J. S. Slaney, Metal Progress, 1964, July, p. 109.

45. H. J. Murphy, C. T. Sims, and A. M. Bettram, J. Metals, 1968, Vol. 20, No. 11, 56.

46. A. Taylor and R. W. Floyd, J. Inst. Met. 80, 577, 1952.

47. P. Duwez and J. L. Taylor, J. Metals 2, 1173, 1950.

48. Gevers, R., Van Landuyt, J., and Amelnckx, S., 1965, Phys. Stat. Sol., 11, 689.

8. FUTURE WORK

1. Further study of the γ' particle growth process on the basis of Lifshits-Wagner theory for the Co-base superalloy should be carried out.
2. The formation mechanism of the metastable ordered phases, Tetragonal $(Co, Ni)_3 Nb$, Cubic $(Co, Ni)_3 (Al, Ti)$ and the effect of solute content (Nb, Ti, Mo, Al) in terms of misfit effect between precipitate and matrix should be investigated in detail.
3. The deformation behaviour of the Co-base superalloy should be studied in order to establish the nucleatian sites for ordered γ' $(Ni_3 Ti)$ and γ'' $(Ni_3 Nb)$ precipitate with mismatch, more than 1.0%.
4. The interfacial structure of γ' with high mismatch (>0.10%) should also be determined.

9. ACKNOWLEDGEMENTS

I would like to express my sincere thanks to Dr. M. C. Chaturvedi whose assistance and guidance made this work possible. I would also like to thank the Mechanical Engineering Department, University of Manitoba, The National Research Council, Ottawa and Centre D'Information Du Cobalt, Brussels, for the financial support.

10. GRAPHS AND DIAGRAMS

Figure 1

Equilibrium phase diagram for precipitation hardenable binary alloy. A metastable miscility gap is denoted by the dashed line.

Figure 2

Typical predicted contrast around spherically symmetrical strained inclusion showing the definition of the 2%, 20%, and 50% image widths. For the operating reflection g indicated, the line of no contrast on a micrograph is as shown.

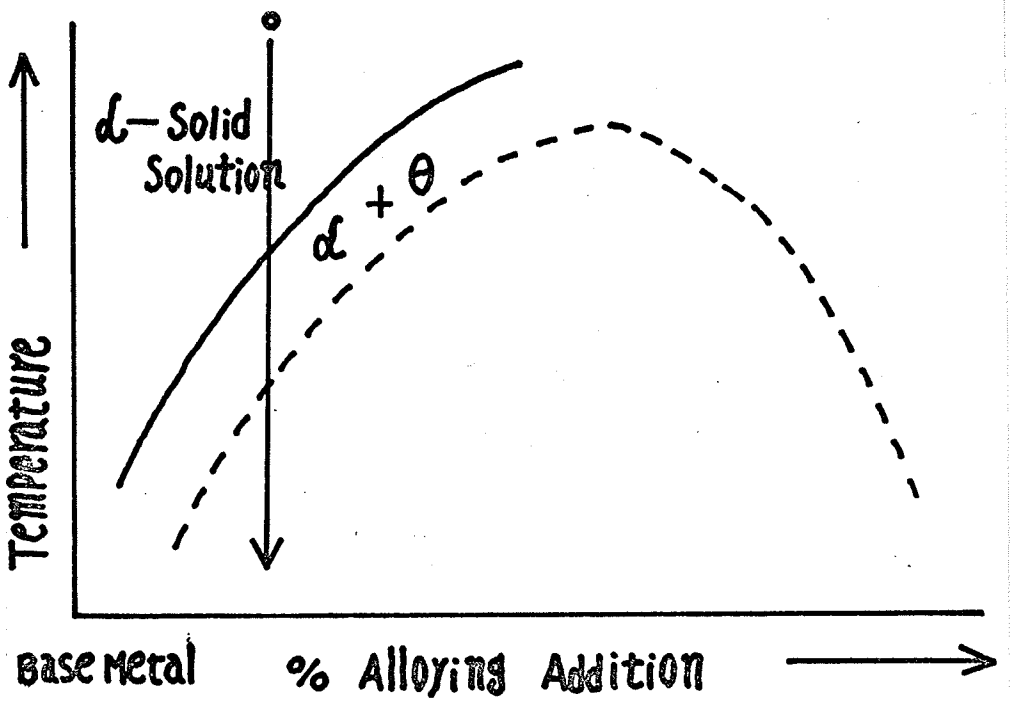
α – Solid Solution
α + θ
Temperature
Base Metal
% Alloying Addition

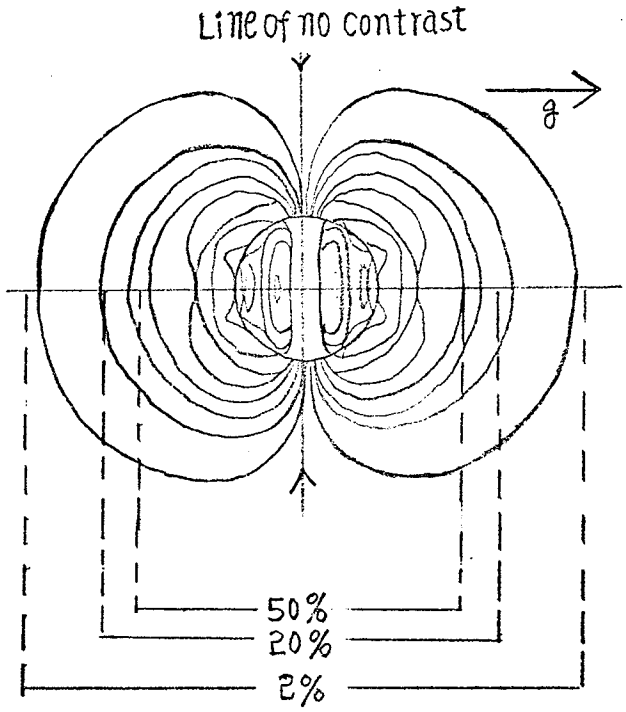
Line of no contrast
g
50%
20%
2%

Figure 3

As-quenched structure of the alloy.

Figure 4

Hardness aging curves at various temperatures.

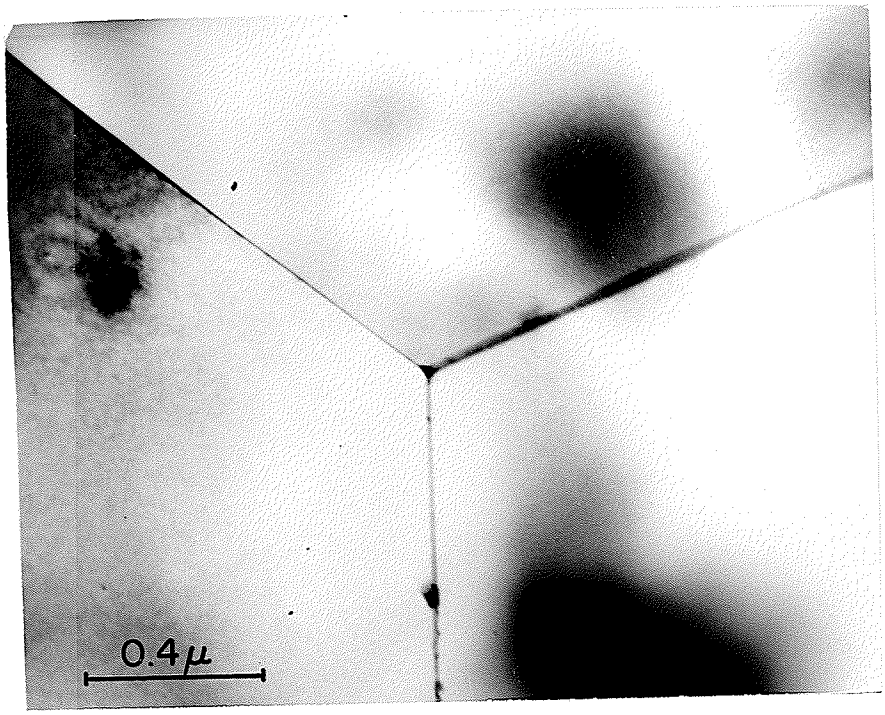
0.4μ

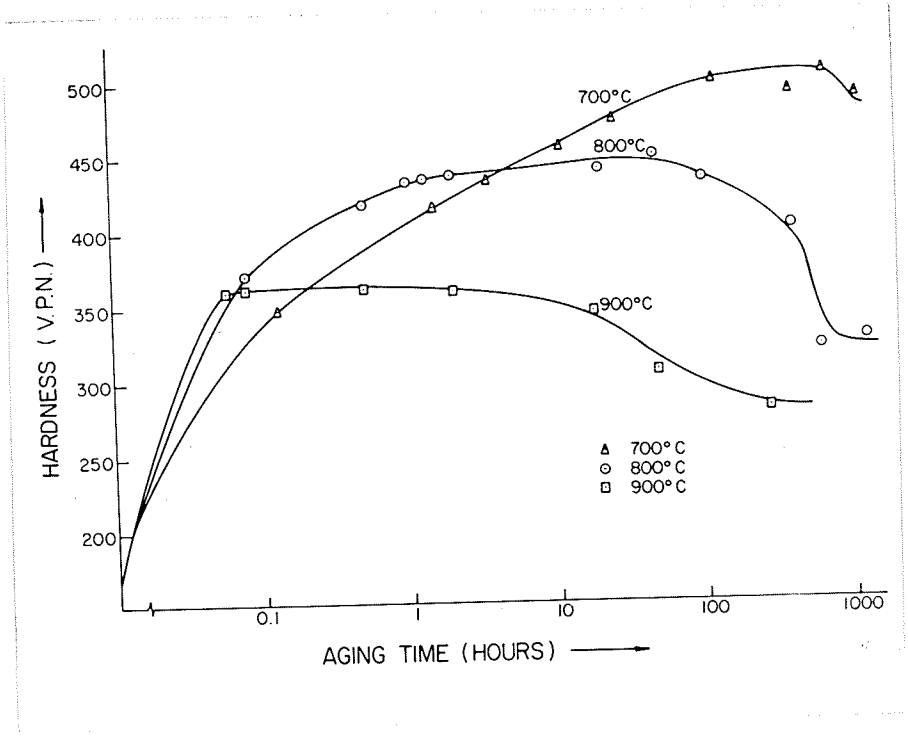
HARDNESS (V.P.N.)
500
450
400
350
300
250
200
700°C
800°C
900°C
700° C
800° C
900° C
0.1
1
10
100
1000
AGING TIME (HOURS)

Figure 5(A)

Thin film structure of the alloy aged for ½ hour at 800°C.

Figure 5(B)

Diffraction pattern of area shown in figure 5(A).

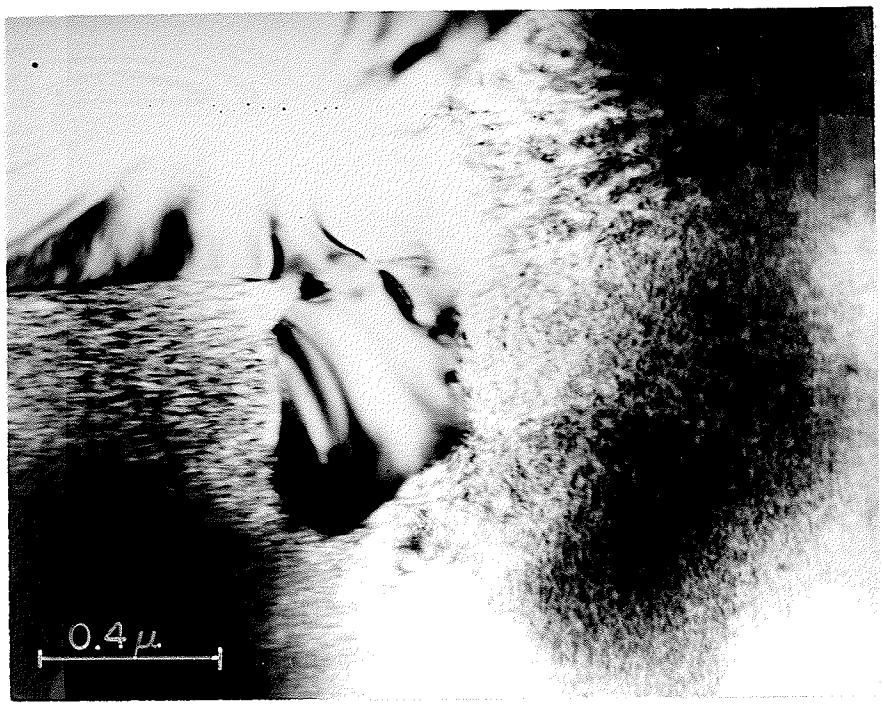
0.4μ

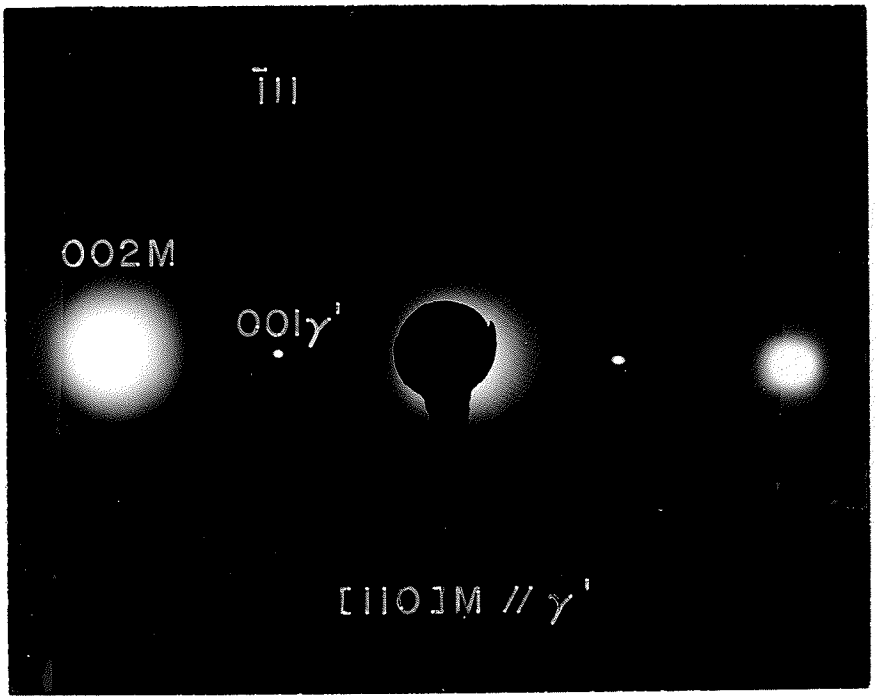
111
002M
001γ'
[110]M // γ'

Figure 6

Dark field structure of a specimen aged for 2 hours at 800°C.

Figure 7

Variation in the lattice parameters of γ and γ'.

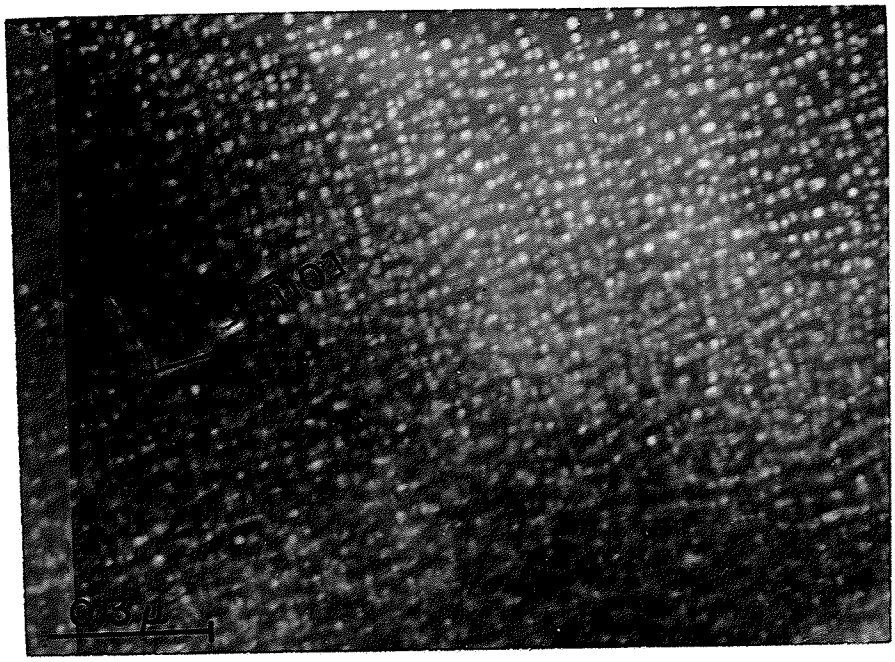
0.3 μ

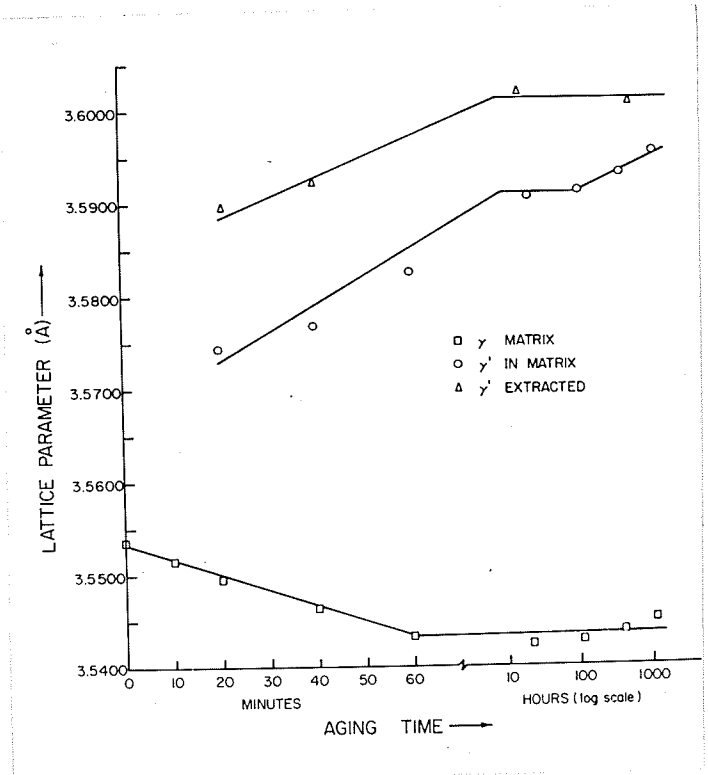
LATTICE PARAMETER (Å)
3.6000
3.5900
3.5800
3.5700
3.5600
3.5500
3.5400
γ MATRIX
γ' IN MATRIX
γ' EXTRACTED
0
10
20
30
40
50
60
10
100
1000
MINUTES
HOURS (log scale)
AGING TIME

Figure 8

Structure of a specimen aged for 575 hours at 800°C.


0.4μ

Figure 9

Bright and dark field picture of stacking faults observed in figure 8.

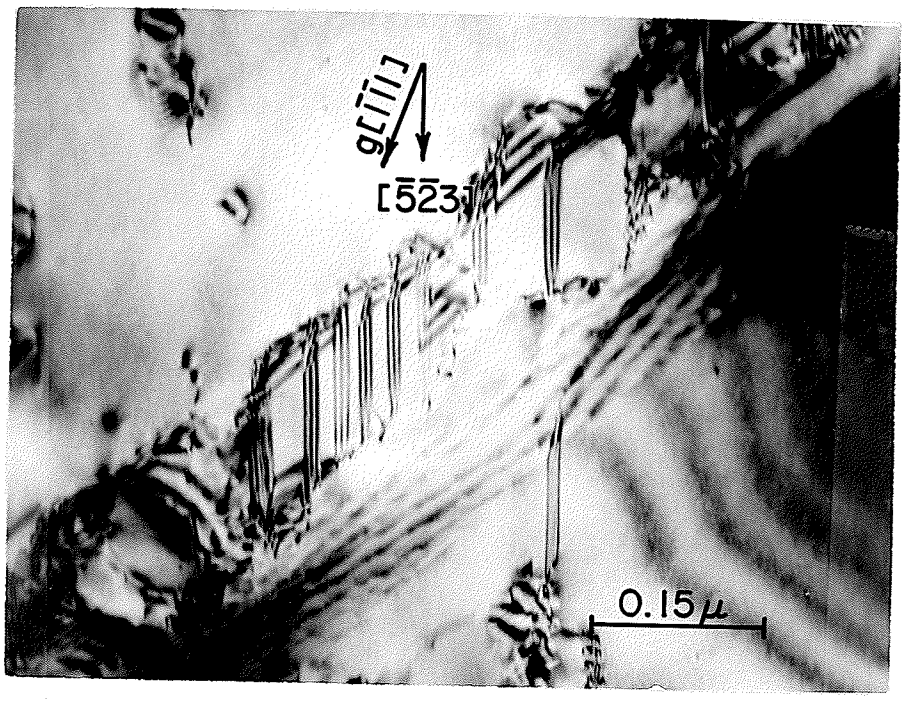
g[111]
[5̄2̄3]
0.15μ

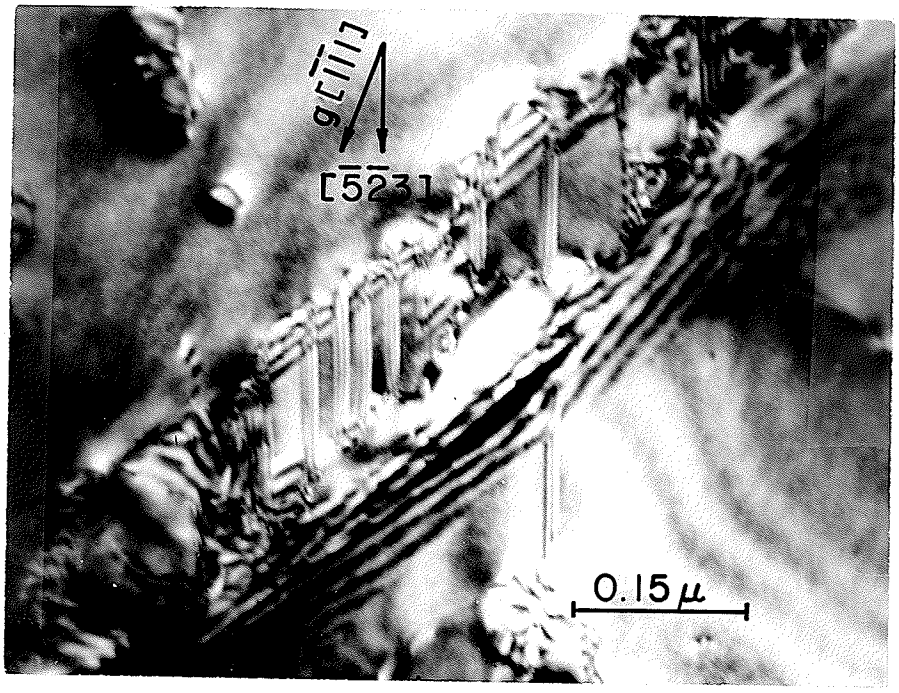
g[1̄11]
[5̄23]
0.15μ

Figure 10

Structure of a specimen aged for 650 hours at 800°C.

Figure 11

Diffraction pattern of figure 10.

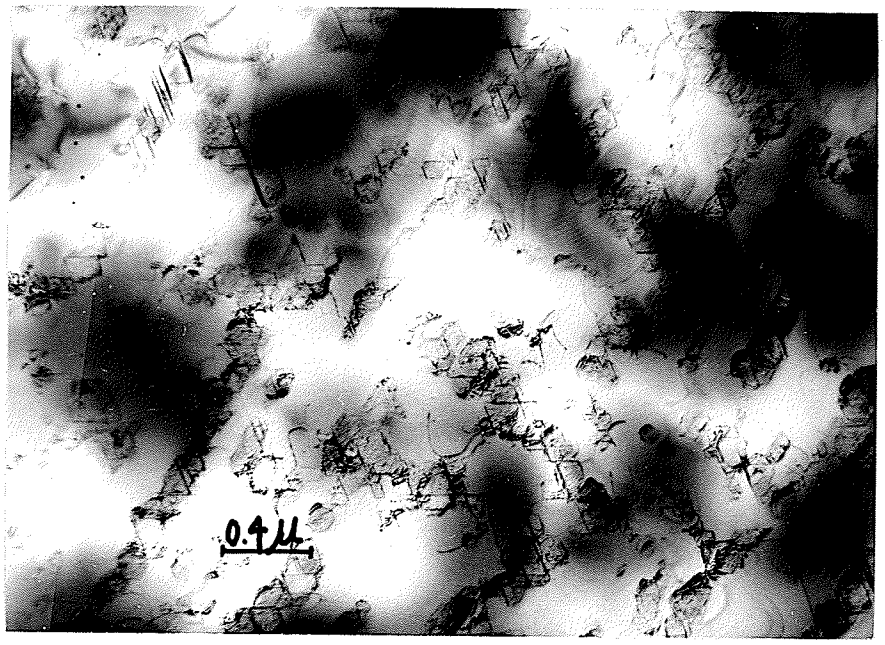
0.4μ

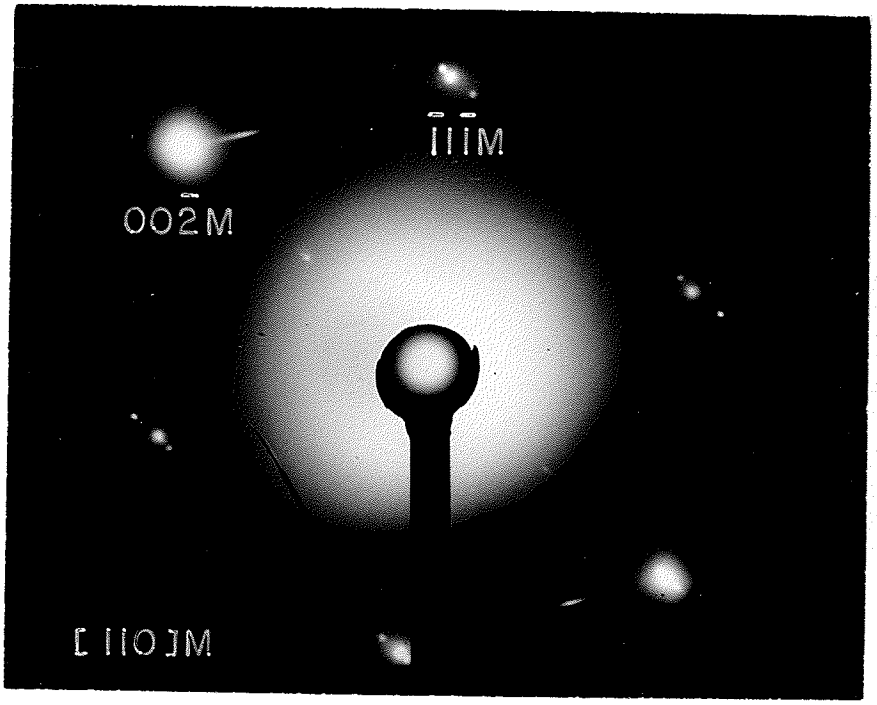
M111
M200
M[011]

Figure 12

Dark field of figure 10 taken with η diffraction spot.

Figure 13

Structure of a specimen aged for 1200 hours at 800°C (carbon extraction replica).

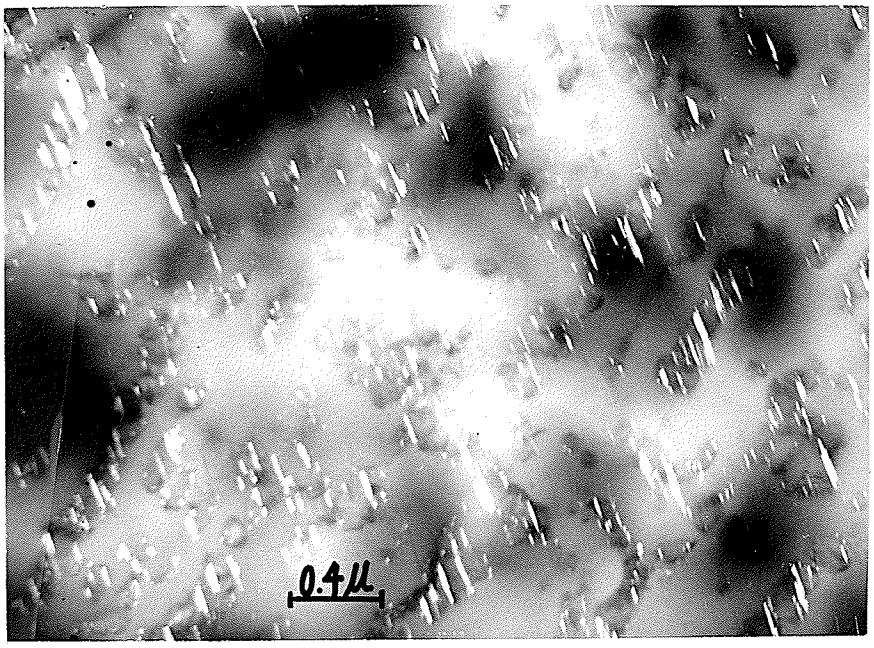
0.4μ


η
γ'
2μ

Figure 14

Diffraction pattern of $M_{23}C_6$ carbide observed at the grain boundary in figure 5(A).

Figure 15

Structure of a specimen aged for ½ hour at 700°C.

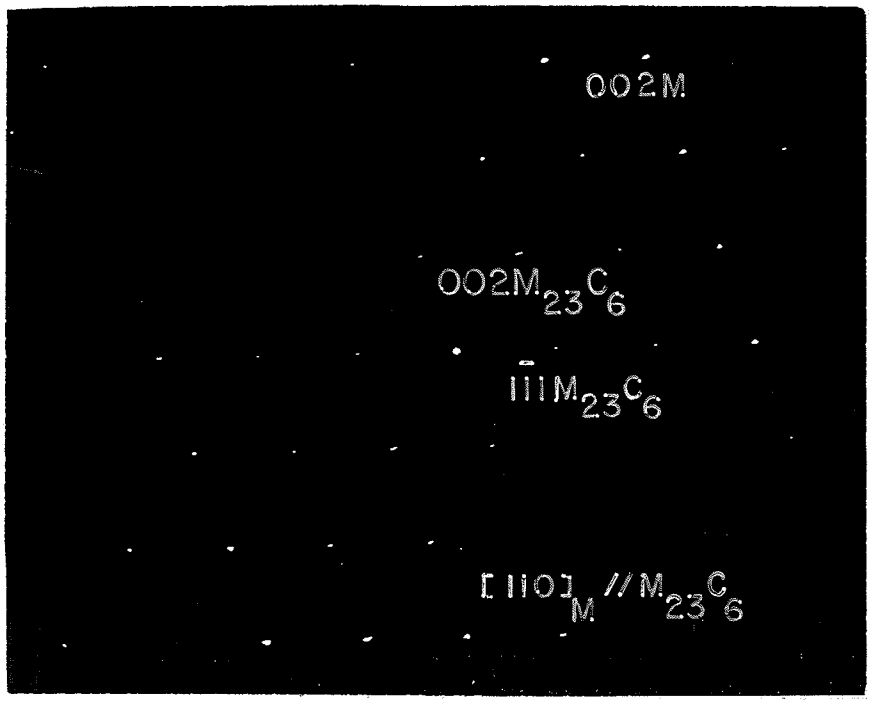
002M
002M23C6
111M23C6
[110]M // M23C6

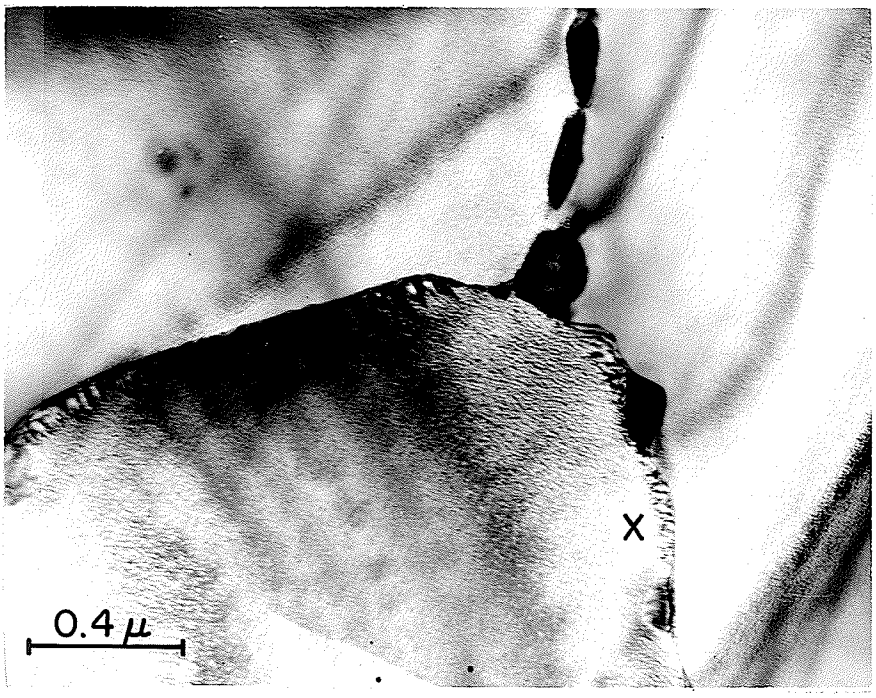
X
0.4 μ

Figure 16

Dark field structure of a specimen aged for 7 hours at 800°C showing TiC precipitate at the grain boundary.

Figure 17

Structure of a specimen aged for 70 hours at 800°C.

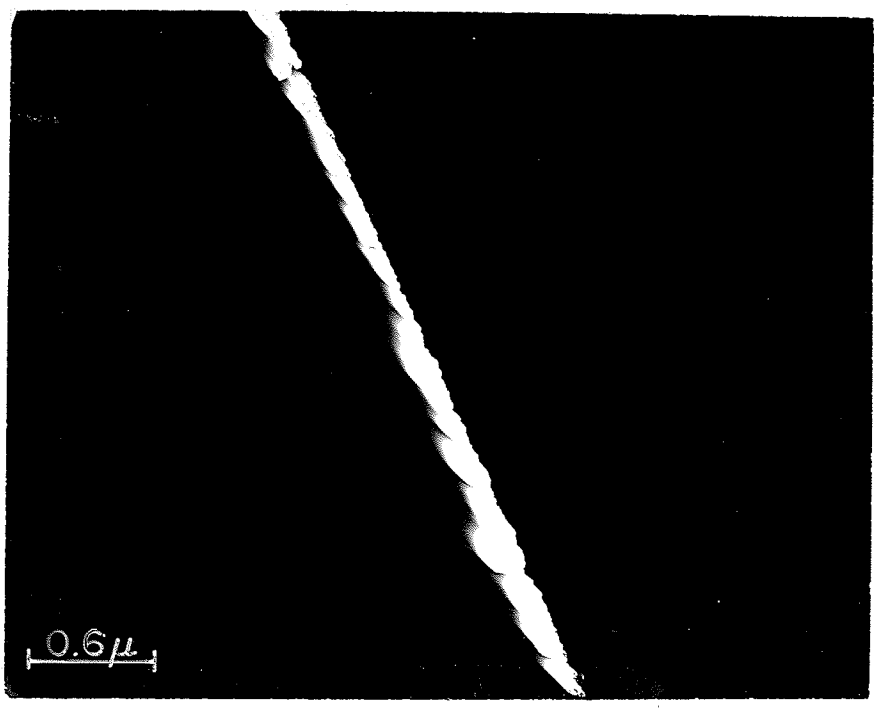
0.6μ

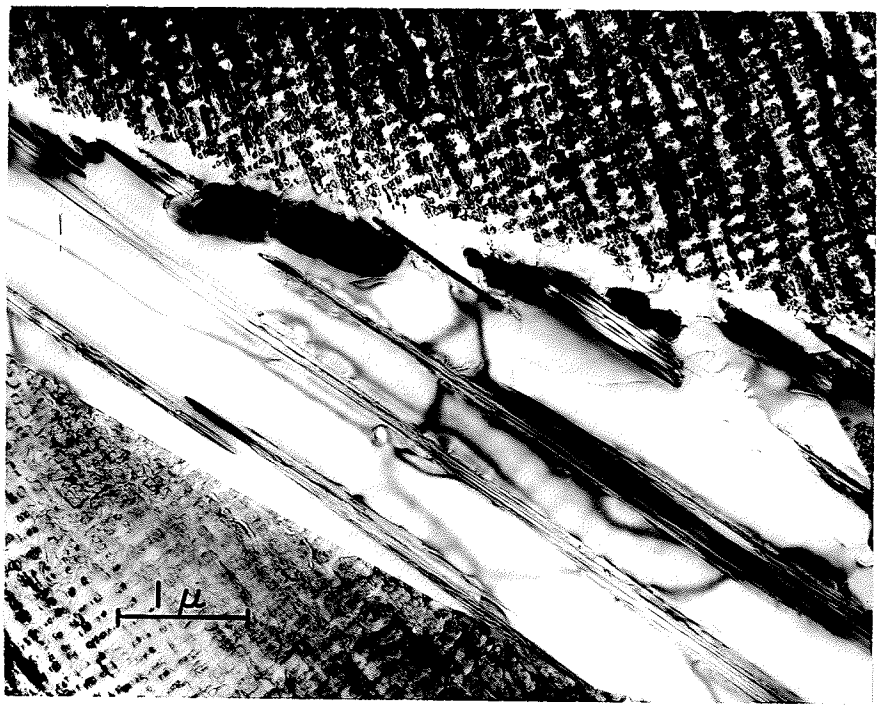
1 μ

Figure 18

Dark field of figure 17 showing η hexagonal phase.

Figure 19

Dark field of figure 17 showing $M_{23}C_6$ carbide.

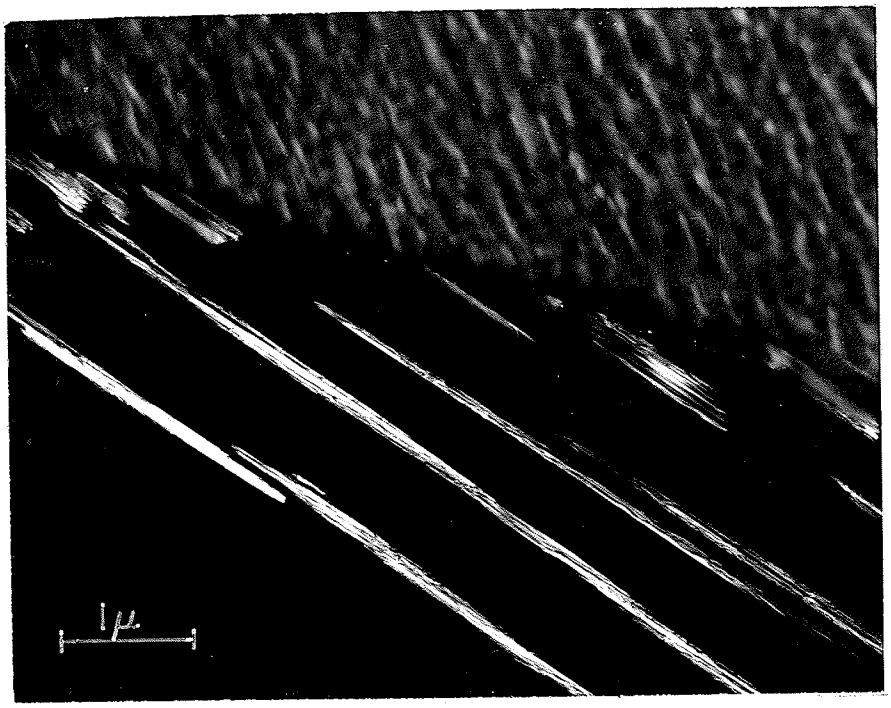
1μ


1μ

Figure 20

Cellular precipitates at the grain boundary of a specimen aged at 800°C.

Figure 21

Diffraction pattern of the area shown in figure 20.

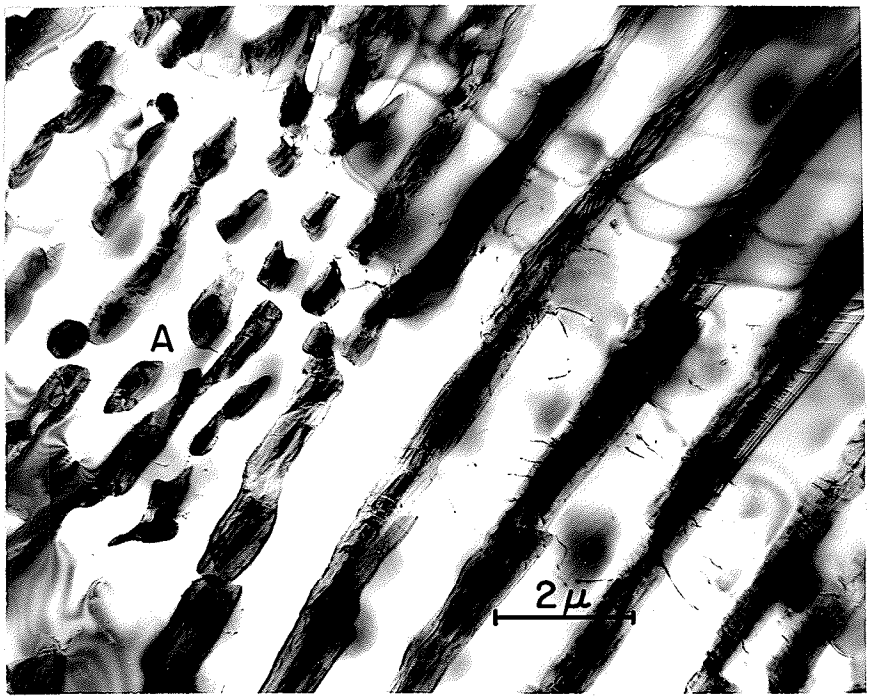
A
2μ

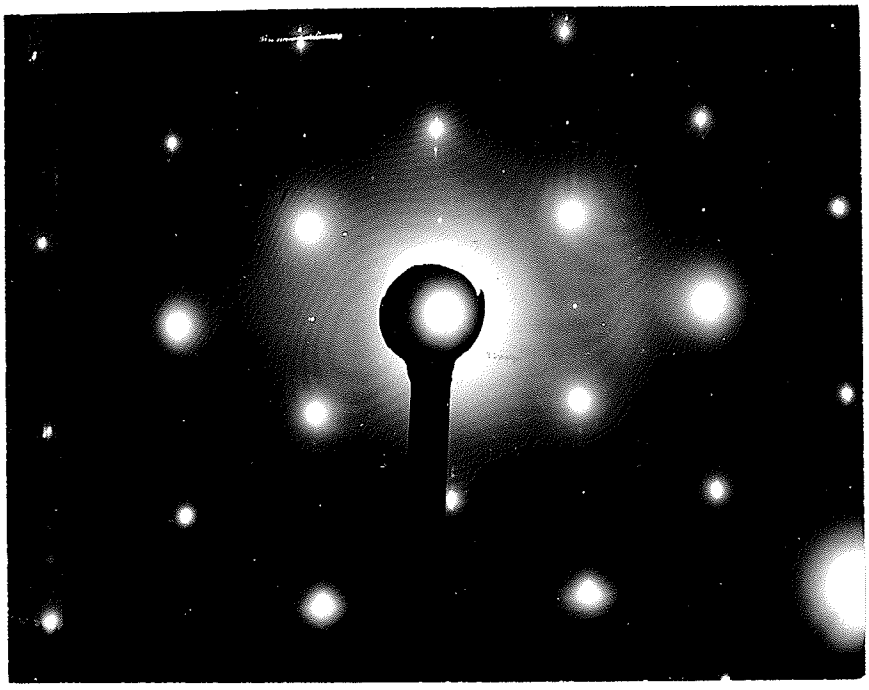

Figure 22

Interpretation of the diffraction pattern shown in figure 21.

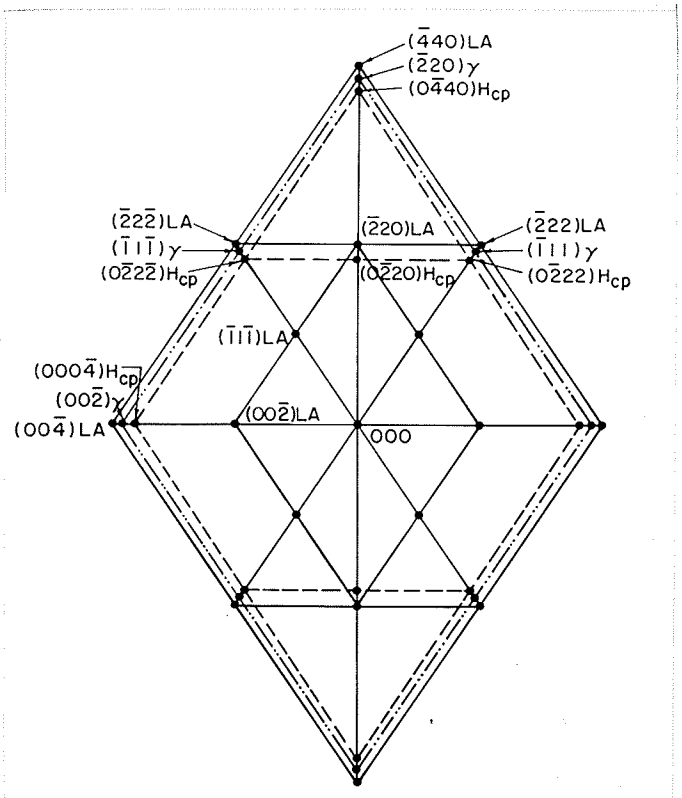

$[110]_\gamma$ // $[10\bar{1}0]$ H_{cp} // $[110]$ Lave, $(Co.Ni)_2Ti$

Figure 23

σ-phase in a specimen aged for 300 hours at 900°C.

Figure 24

Diffraction pattern of σ-phase observed in figure 23.


1 μ

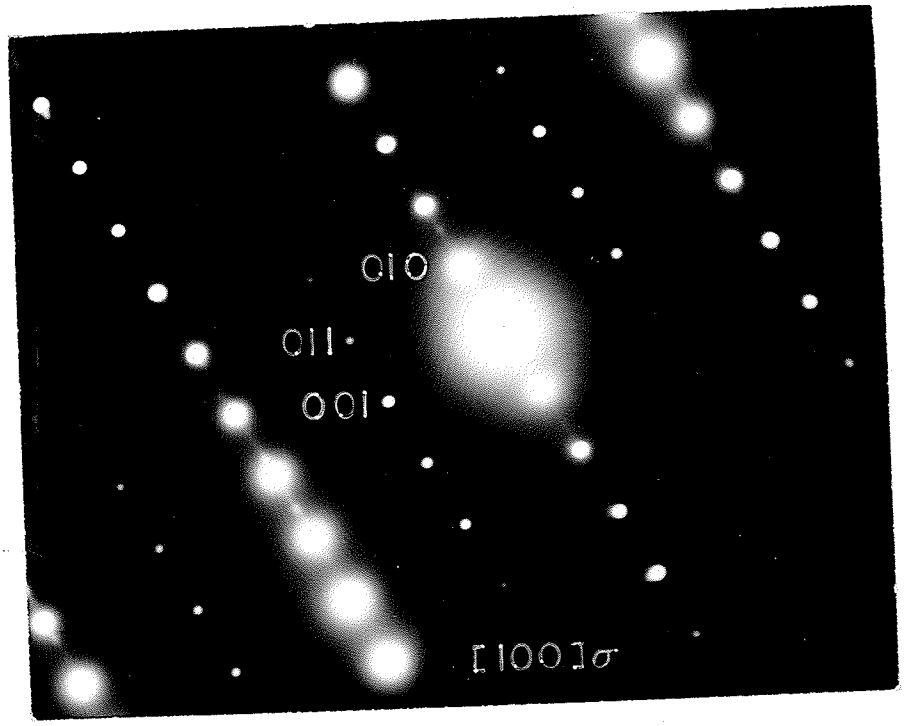
010
011
001
[100]σ

Figure 25

Cubic γ' particles from a carbon extracted replica, aged for 47 hours at $900^{o}C$. Magnification x 97,200.

TABLE OF PHASES OCCURRING AT VARIOUS STAGES OF AGING

Temp.	At or Near Grain-boundaries			Within the Grains		
	Phase	Structure	Lattice Parameter	Phase	Structure	Lattice Parameter
$700^{o}C$	Carbide (TiC)	F.C.C.	a= 4.286Å	γ' $(Co.Ni)_3Ti$	ordered F.C.C.	a= 3.594Å
	Carbide $(M_{23}C6)$	F.C.C.	a=10.659Å	η (Ni_3Ti)	ordered H.C.P.	a= 5.122Å
	η (Ni_3Ti)	ordered H.C.P.	a= 5.122Å c= 8.242Å			c= 8.242Å
$800^{o}C$	Carbide (TiC)	F.C.C.	a= 4.286Å	γ' $(Co.Ni)_3Ti$	ordered F.C.C.	a= 3.594Å
	Carbide $(M_{23}C6)$	F.C.C.	a=10.659Å	η (Ni_3Ti)	ordered H.C.P.	a= 5.122Å c= 8.242Å
	η (Ni_3Ti)	ordered H.C.P.	a= 5.122Å c= 8.242Å			
	Lave $(Co.Ni)_2Ti$	ordered F.C.C.	a= 7.15Å			
$900^{o}C$	Carbide (TiC)	F.C.C.	a= 4.286Å	γ' $(Co.Ni)_3Ti$	ordered F.C.C.	a= 3.594Å
	Carbide $(M_{23}C6)$	F.C.C.	a=10.659Å	η (Ni_3Ti)	ordered H.C.P.	a= 5.122Å c= 8.242Å
	η (Ni_3Ti)	ordered H.C.P.	a= 5.122Å c= 8.242Å			
	σ (Co-Cr)	B.C.T.	a= 8.40Å c= 4.48Å